APL Photonics

# Near-field hyper-spectral imaging of resonant Mie modes in a dielectric island

Cite as: APL Photonics **6**, 126102 (2021); https://doi.org/10.1063/5.0070626
Submitted: 08 September 2021 • Accepted: 21 November 2021 • Accepted Manuscript Online: 21 November 2021 • Published Online: 06 December 2021

Nicoletta Granchi, Michele Montanari, Andrea Ristori, et al.

openaccess

View Online Export Citation CrossMark

ARTICLES YOU MAY BE INTERESTED IN

Low-threshold power and tunable integrated optical limiter based on an ultracompact $VO_2$/Si waveguide
APL Photonics **6**, 121301 (2021); https://doi.org/10.1063/5.0071395

Plasma reflectivity behavior under strong subpicosecond excitation of liquids
APL Photonics **6**, 126101 (2021); https://doi.org/10.1063/5.0070963

Projection-suspended stereolithography 3D printing for low-loss optical hydrogel fiber fabrication
APL Photonics **6**, 121302 (2021); https://doi.org/10.1063/5.0067486

Learn more and submit
APL Photonics
Applications now open for the
Early Career Editorial Advisory Board

AIP Publishing



© 2021 Author(s).

# Near-field hyper-spectral imaging of resonant Mie modes in a dielectric island

Cite as: APL Photon. 6, 126102 (2021); doi: 10.1063/5.0070626
Submitted: 8 September 2021 • Accepted: 21 November 2021 •
Published Online: 6 December 2021

View Online Export Citation CrossMark

Nicoletta Granchi,[1,2,a] Michele Montanari,[1,2] Andrea Ristori,[1] Mario Khoury,[3] Mohammed Bouabdellaoui,[3] Chiara Barri,[4,5] Luca Fagiani,[4,5] Massimo Gurioli,[1,2] Monica Bollani,[4] Marco Abbarchi,[3] and Francesca Intonti[1,2]

## AFFILIATIONS

[1] LENS, University of Florence, Sesto Fiorentino 50019, Italy
[2] Department of Physics and Astronomy, University of Florence, Sesto Fiorentino 50019, Italy
[3] Aix Marseille Univ, Université de Toulon, CNRS, IM2NP, Marseille, France
[4] Istituto di Fotonica e Nanotecnologie (IFN)-Consiglio Nazionale delle Ricerche, Laboratory for Nanostructure Epitaxy and Spintronics on Silicon, Via Anzani 42, 22100 Como, Italy
[5] Department of Physics, Politecnico di Milano, Piazza Leonardo Da Vinci 32, 20133 Milano, Italy

[a] **Author to whom correspondence should be addressed:** granchi@lens.unifi.it

## ABSTRACT

All-dielectric sub-micrometric particles have been successfully exploited for light management in a plethora of applications at visible and near-infrared frequencies. However, the investigation of the intricacies of the Mie resonances at the sub-wavelength scale has been hampered by the limitations of conventional near-field methods. In this paper, we address the spatial and spectral mapping of multipolar modes of a Si island by hyper-spectral imaging. The simultaneous detection of several resonant modes allows us to clarify the role of the substrate and the incidence angle of the impinging light, highlighting spectral splitting of the quadrupolar mode and resulting in different spatial features of the field intensity. We explore theoretically and experimentally such spatial features. Details as small as 200 nm can be detected and agree with simulations based on the finite difference time domain method. Our results are relevant to near-field imaging of dielectric structures, the comprehension of the resonant features of sub-micrometric Mie antennas, beam steering, and the resonant coupling with light emitters. Our analysis suggests a novel approach to control the absorption of a single emitter in the framework of surface enhanced absorption or stimulated emission applications.

*© 2021 Author(s). All article content, except where otherwise noted, is licensed under a Creative Commons Attribution (CC BY) license (http://creativecommons.org/licenses/by/4.0/).* https://doi.org/10.1063/5.0070626

## I. INTRODUCTION

All-dielectric sub-wavelength sized Mie resonators have emerged in the last decade as promising building blocks for opto-electronic devices, since they provide the possibility to efficiently redirect and concentrate light with low absorption losses.[1] The optical modes in high-index dielectric nanoparticles originate from the excitation of optically induced displacement currents and can be both magnetic and electric in nature. The combination of these two kinds of resonant modes and the exploitation of higher order multipolar modes offer opportunities for directional and polarization-controlled emission from nanoemitters.[2–6] Moreover, in the field of light–matter interaction, high refractive index dielectric nanoparticles have recently been considered as a possible alternative to metallic nanoparticles for generating localized optical resonances down to nanoscale. In fact, the concentration of light in subwavelength hotspots represents an essential element for surface enhanced fluorescence[7] and for manipulating the generation of nonclassical light by quantum emitters.[8]

For these purposes, a complete knowledge of the electric and magnetic nature of the modes, their spectral features, and their spatial distribution is mandatory. Finite difference time domain (FDTD) numerical calculations represent a powerful tool to systematically study the resonant properties of high-index dielectric


© Author(s) 2021

particles.[9–11] However, the direct experimental characterization of these peculiarities has almost exclusively dealt with far-field measurements[12,13] that do not provide access to the spatial distribution of the resonant modes.

Sub-wavelength spatial resolution imaging has been realized in the past by cathodoluminescence imaging spectroscopy[14] or apertureless (scattering-type) near-field scanning optical microscopy.[15–17] A similar approach based on scattering-type near-field microscopy was efficiently exploited for mapping the near-field features of plasmonic resonances formed in gold-based rods,[18] gap antennas,[19] and meta-molecules,[20] allowing us also to retrieve the phase of the scattered field. However, these methods are either limited to the collection of the signal in dielectric regions, i.e., only in the small area covered by the sub-wavelength sized Mie resonators,[14] or do not provide information on more than one optical mode at a time owing to the use of a laser at a fixed frequency, thus disregarding also the essential aspects of the compresence of spectral and spatial features of the investigated structures.

Here, we present via near-field hyper-spectral imaging (HSI) a detailed sub-wavelength optical characterization of the multipolar resonances formed in a monocrystalline silicon island, simultaneously providing spectral and spatial information on several resonances in a single measurement. Experimental results are explained and validated by FDTD simulations.[21] Exploiting the etalon effect springing from the thick $SiO_2$ layer between the antenna and the bulk Si substrate underneath, we detect the splitting of one resonance into sharper peaks, unraveling the difference and intimate features of their near-field details. We thus achieve a complete understanding of the effect of the substrate on the resonant modes, filling a gap in a research field that so far has considered the presence of the substrate mostly as a strong limitation of the Mie resonator properties. We also show that intensity and spatial light localization in the near-field strongly depend on the illumination angle, clarifying the crucial role of the excitation configuration that can be exploited as a spatial tuning tool to control, through the electric field intensity maxima induced by external illumination on the antenna, the absorption of a single emitter in close proximity.

The possibility of characterizing the near-field of higher order multipolar modes, such as the magnetic quadrupole (MQ) that in this case is split into three resonances, thanks to the presence of the etalon, fills a gap in the previous works that were often focused on low order Mie resonances. The ability to identify in Si islands the resonances with magnetic nature can be exploited to promote the magnetic radiative decay in quantum emitters with forbidden dipole transitions, such as trivalent lanthanide ions that undergo magnetic spontaneous emission.[22] Mie resonators characterized by a relatively high-quality factor and negligible Ohmic losses are a very attractive approach to promote magnetic emission in quantum emitters, which represents an important step toward the realization of bright magnetic emitters at optical frequencies.[23]

## II. EXPERIMENT

The investigated samples consist of monocrystalline Si-based islands fabricated via low-resolution optical lithography and plasma etching followed by solid state dewetting.[24–27] A 2 $\mu$m thick layer of $SiO_2$ separates the islands from an underlying bulk Si substrate. Details on the fabrication process can be found in Refs. 25–27. In

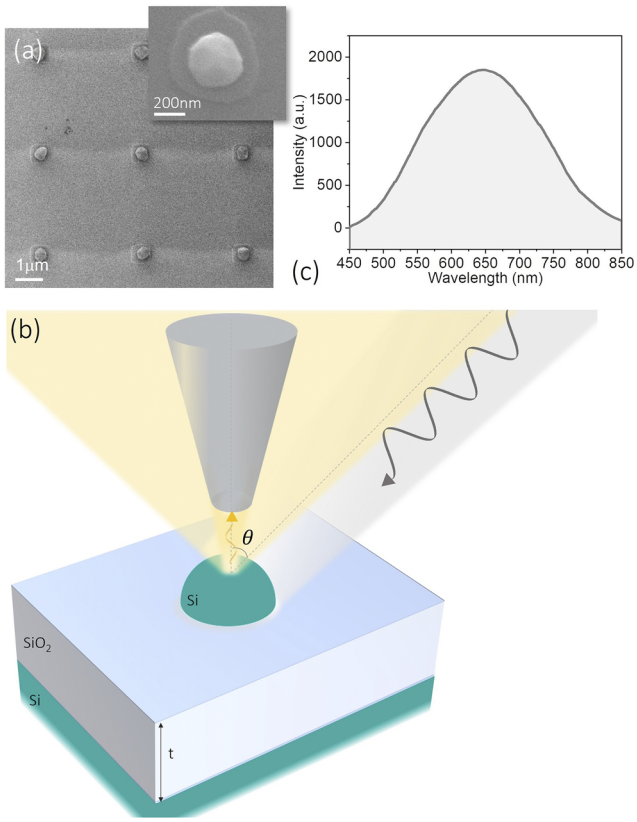


**FIG. 1.** (a) Top view of the SEM image of the sample in which several dewetted islands are shown. The inset displays the magnified SEM image of a single island. (b) Sketch of the experimental setup: the tilted illumination (of an angle $\theta$ with respect to the axis perpendicular to the sample) from the supercontinuum is scattered by the island. The yellow cone is a representation of the angular pattern of scattering. The scattered light is collected by the near-field tip at a distance of ≈10 nm from the sample surface. (c) Emission spectrum of the supercontinuum source detected by a Si-based CCD camera.

Fig. 1(a), we report a top view Scanning Electron Microscopy (SEM) image of the sample showing several dewetted islands; the details of a single island with a diameter of the order of 300 nm can be observed in the SEM image in the inset of Fig. 1(a).

A scanning near-field optical microscope (SNOM) in collection geometry was used in order to detect the near-field scattered emission of a single island in a tilted illumination configuration [as shown in Fig. 1(b)]. A complete description of the experimental setup can be found in Sec. S1 of the supplementary material. The spatially resolved optical maps were recorded by scanning the probe (a dielectric tip) over the sample at a fixed distance (few tens of nanometers). The SNOM probe is a silica-based optical fiber chemically etched. The illumination source, shined at an angle of incidence of $\theta = 30^\circ$ with respect to the axis perpendicular to the substrate, is a supercontinuum laser, whose scattering spectrum, collected with the cooled Si-based CCD camera used in the experiment, is reported in Fig. 1(c). The signal is fed with a 10 cm focal length achromatic lens into a spectrometer and detected by the CCD camera. At every tip


© Author(s) 2021

position, the entire spectrum of the sample is collected with a spectral resolution of 0.4 nm. This technique allows us to perform HSI by collecting a full near-field spectrum at every tip position of the spatial map.

## III. THEORETICAL SIMULATIONS: MODE EVOLUTION WITH SUBSTRATE AND ANGLE OF ILLUMINATION

We study the modification on the scattering spectra of a single Si-based scatterer as a function of the thickness t of the $SiO_2$ substrate and the illumination angle $\theta$ by means of FDTD simulations with a commercial software lumerical .[21] We consider a hemispherical Si island of diameter d = 330 nm [Fig. 2(a)] illuminated by a Total Field Scattered Field (TFSF) source, which launches a broadband ($\lambda$ = 400–1200 nm) plane wave from the top and filters out all the light that has not been scattered. The simulated source is polarized along the x axis and can be tilted by an angle $\theta$ with respect to the z axis. Power transmission monitors are positioned around the TFSF source in order to obtain the total scattering cross section, and two field monitors intersect the particle (along the xz and yz plane) to monitor the local field intensity. An additional monitor is placed on top of the island in the xy plane at a distance of 10 nm from the apex in order to simulate the near-field spatial profile of the electric field intensity. Perfectly Matching Layers (PMLs) are used to prevent unphysical scattering from the simulation boundaries and to mimic semi-infinite substrates. Optical constants for Si and $SiO_2$ are taken from the work of Palik.[28]

Figure 2(b) reports the total scattering cross sections of the Si hemisphere, illuminated under normal incidence, for different values of the substrate thickness t. In particular, it is possible to follow the evolution of the modes from the case of the island in air (yellow spectrum) to the configuration with the maximal $SiO_2$ thickness of 2 $\mu$m (blue spectrum). The latter is the actual value of t in the experimentally investigated sample. The scattering cross sections for three selected values of t (i.e., t = 25, 500, and 1300 nm), are reported in Fig. 2(b) in orange, magenta, and purple, respectively. The identification of these modes [electric hexapole (EH), magnetic hexapole (MH), electric quadrupole (EQ), magnetic quadrupole (MQ), and electric and magnetic dipole (ED/MD)], which are reported in Table I, is based on their field intensity profile inside the particle and the corresponding current loops [Fig. 2(c)].

First, electric and magnetic field intensity inside the hemisphere suspended in air allows us to identify the multipolar resonances from the fundamental to higher-energy ones. In the near-field, the electric (magnetic) field profiles in the xz (yz) plane for electric (magnetic) resonances show bright lobes inside, corresponding to the poles generated by current loops [white arrows in Fig. 2(c)]. The number of

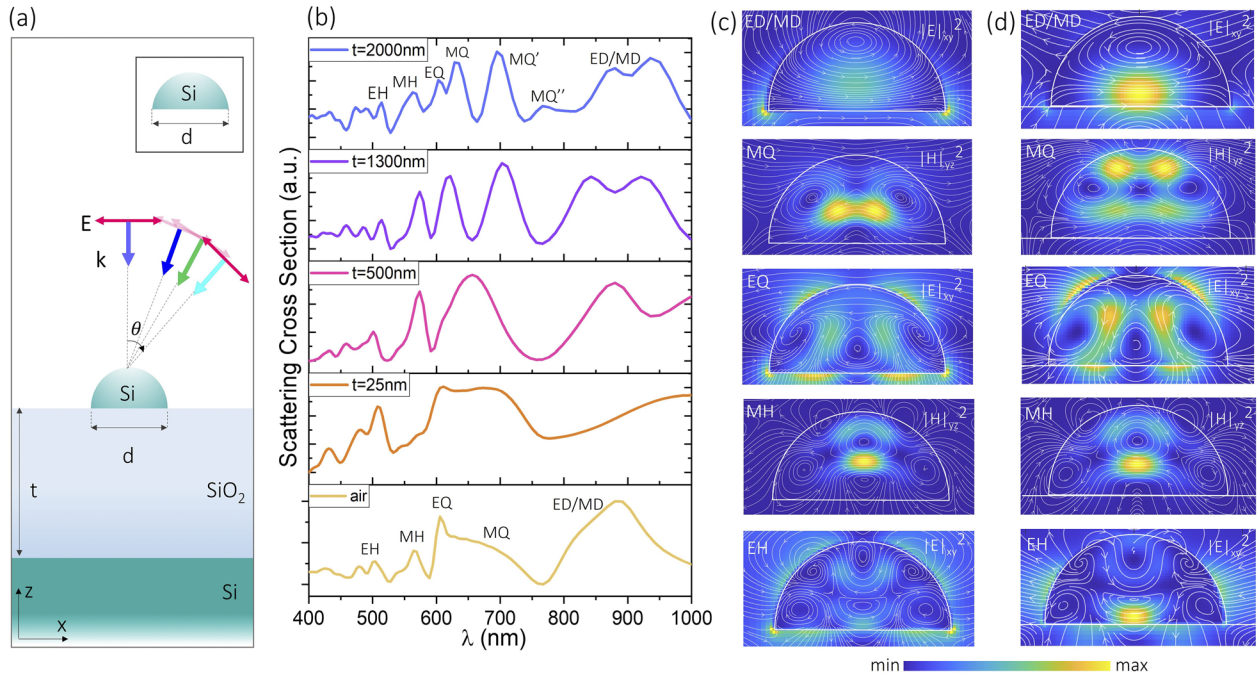


**FIG. 2.** (a) Sketch of the model used in the FDTD simulations; a Si hemisphere of diameter d is positioned atop a $SiO_2$ layer of thickness t and a bulk Si substrate. The scatterer is illuminated by an x polarized TFSF source that can be tilted by an angle $\theta$ with respect to the z axis. The inset shows the bare case of the island in air. (b) FDTD scattering cross sections (from bottom to top) for increasing values of t, t = 0 (island in air), t = 25, 500, and 1300 nm, respectively, in yellow, orange, magenta, and purple. (c) Vertical crosscuts of the electromagnetic field intensity and current loops (represented by white arrows) of the multipolar resonances of the hemisphere in air. The maps, acquired at the wavelengths of the yellow spectrum, are reported from top to bottom in the order of increasing energy: ED/MD ($\lambda$ = 920 nm), MQ ($\lambda$ = 660 nm), EQ ($\lambda$ = 605 nm), MH ($\lambda$ = 570 nm), and EH ($\lambda$ = 504 nm). (d) Vertical crosscuts of the electromagnetic field intensity and current loops (represented by white arrows) of the multipolar resonances of the hemisphere on a $SiO_2$ layer of thickness t = 2 $\mu$m. The maps, acquired at the wavelengths of the blue spectrum, are reported from top to bottom in the order of increasing energy: ED/MD ($\lambda$ = 906 nm), MQ ($\lambda$ = 628 nm), EQ ($\lambda$ = 603 nm), MH ($\lambda$ = 563 nm), and EH ($\lambda$ = 514 nm).


© Author(s) 2021

**TABLE I.** Table in which we report all the Mie resonances found for the case of the island with d = 330 nm in air and on a thick substrate (t = 2000 nm). For each mode, we report the number of poles inside the electromagnetic field distributions in the vertical crosscuts.

| | Number of poles | Island in air | Island on thick $SiO_2$ (t = 2 $\mu$m) |
|---|---|---|---|
| ED/MD | 1 | $\lambda$ = 920 nm | $\lambda$ = 906 nm |
| | | | MQ″ $\lambda$ = 766 nm |
| MQ | 4 | $\lambda$ = 660 nm | MQ′ $\lambda$ = 695 nm |
| | | | MQ $\lambda$ = 628 nm |
| EQ | 4 | $\lambda$ = 605 nm | $\lambda$ = 603 nm |
| MH | 6 | $\lambda$ = 570 nm | $\lambda$ = 563 nm |
| EH | 6 | $\lambda$ = 504 nm | $\lambda$ = 514 nm |

poles is reported for each mode in the first column of Table I. The effects of symmetry breaking with respect to the ideal case of a sphere in air (in which ED and MD are easily distinguishable) must be considered[29,30] and are beyond the scope of this paper. We therefore refer to the broadband centered around 900 nm as ED/MD. The criterion used to choose the ED/MD crosscut is explained in Sec. S2 of the supplementary material. We also identify the main higher-order resonances as MQ, EQ, MH, and EH, of which we report the vertical crosscuts of E or H, respectively, at $\lambda$ = 660, 605, 570, and 504 nm.

The same reasoning was adapted to assign the resonances of the particle sitting atop a $SiO_2$ substrate while t increases. It was recently shown[9,25] that by increasing t, constructive and destructive interference of the incident light reflected from the $SiO_2$/Si-bulk interface arises, resulting in strong variations in the driving field of the resonator. The Mie scattering efficiently out-couples the light interfering in the etalon and redirects light at smaller angles with respect to the incident beam. From this combination, structural colors spring, covering the full visible spectrum with resonances with a high intensity contrast between maxima and minima. However, a detailed identification of the actual physical origin of these sharp peaks has never been attempted so far.

While increasing t, we can follow the evolution of the vertical profiles of the electric (magnetic) field intensity along the xz (yz) plane of the main electric (magnetic) resonances in the scatterer [Fig. 2(d) for the main resonances of the blue spectrum on top of Fig. 2(b) corresponding to the nominal $SiO_2$ thickness t = 2 $\mu$m]. Specifically, the maps of ED/MD, MQ, EQ, MH, and EH correspond to $\lambda$ = 906, 628, 603, 563, and 514 nm, respectively.

The original broadband corresponding to MQ in the yellow spectrum (scatterer in air) splits into three sharp peaks, all identifiable as magnetic quadrupole resonances from the analyzed current loops, to which we refer to as MQ, MQ′, and MQ″ (more details are given in Fig. S3 of the supplementary material). The list of all the modes arising for t = 2 $\mu$m can be found in the third column

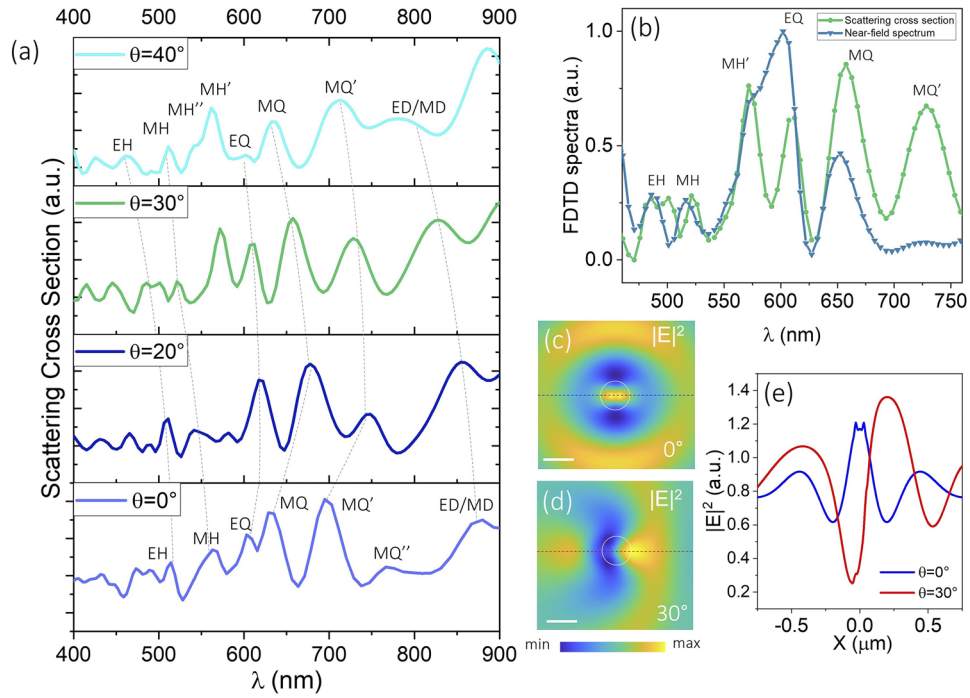


**FIG. 3.** (a) FDTD scattering cross sections for different angles of illumination, from bottom to top: $\theta$ = 0° in blue, $\theta$ = 20° in dark blue, $\theta$ = 30° in green, and $\theta$ = 40° in cyan. (b) FDTD scattering cross sections in green and FDTD near-field spectrum in dark green acquired on the center of a field monitor at a distance of 10 nm from the hemisphere surface for $\theta$ = 30°. The peaks are labeled according to the identification of the multipolar resonances under tilted illumination EH, MH, MH′, EQ, MQ, and MQ′. (c) and (d) Near-field FDTD spatial distribution of the electric field intensity of MQ for $\theta$ = 0° and $\theta$ = 30°. The white scale bar corresponds to 200 nm. (e) Horizontal cuts of the near-field $|E|^2$ along the blue (red) dashed lines displayed in (c) and (d).


© Author(s) 2021

of Table I. The coupling between the scatterer and the interference arising from the $SiO_2$ layer, combined with the analysis of crosscuts of the electric/magnetic field for every peak, therefore allows us to identify the modes and obtain information about the multipole characteristics of the island spectrum without any needs of multipolar decomposition.[15]

An analog method of identification is used in order to monitor the changes in the scattering properties of the island with respect to the angle of illumination [Fig. 3(a)]. We compute the FDTD scattering cross sections of a Si hemisphere for the t = 2 $\mu$m layer of $SiO_2$ and Si bulk for different angles of illumination $\theta$: the spectra are displayed in blue for $\theta = 0°$, in dark blue for $\theta = 20°$, in green for $\theta = 30°$, and in cyan for $\theta = 40°$. The peaks arising from the coupling of the Mie modes with the etalon are sensible to the angle of illumination, differently with respect to the scattering cross section of the island on a thin substrate that is practically unchanged for different $\theta$ (as shown in Fig. S4 of the supplementary material).

In fact, the broad MH and MQ peaks split due to interference with the etaloning resonances in which the angle of incidence plays a fundamental role. Specifically, for $\theta = 30°$, a second MH appears around $\lambda = 576$ nm (which we call MH′), and one of the three MQs is suppressed, leaving only MQ and MQ′ at $\lambda = 657$ nm and $\lambda = 725$ nm.

We now focus on the scattering in near-field; in Fig. 3(b), we report in dark green the FDTD near-field spectrum acquired at the center of the island for $\theta = 30°$ and the calculated scattering cross section for the same angle of illumination. The two spectra display almost the same resonances but with different relative weights of the peaks; in the near-field, the peaks MH′ and EQ broaden, and as a consequence, they tend to overlap. Provided the high sensitivity of the Mie resonances to large values of t, we analyze through FDTD simulations the near-field spatial profile of the electric field intensity, achieving a fairly good comprehension of the scatterer's responses in such a specific configuration. The near-field distributions of the resonances are strongly affected by the illumination direction. In Figs. 3(c) and 3(d), the near-field FDTD maps of the electric field intensity of the MQ′ mode generated under normal incidence (0°) and tilted incidence (30°) are shown, respectively. In the latter case, the electric field intensity is not symmetrically distributed around the scatterer, and we clearly observe that the hotspot changes its shape and spatially shifts to the right. The shift is of about 250 nm, as highlighted in Fig. 3(e), where the horizontal crosscuts through the center of the maps are compared (respectively, in blue and red). These crosscuts show that also the maximum electric field intensity is influenced by the illumination angle. Figures 3(c)–3(e) show that by changing the illumination angle by 30° on the left half of the Si island, the signal intensity drops from bright to dark, while in the region around the right border of the island, we observe a net increase in the electric field intensity.

## IV. NEAR-FIELD HYPER-SPECTRAL IMAGING EXPERIMENT

In the following, we provide a detailed near-field HSI analysis of the higher order multipolar modes in a single all-dielectric nanoparticle. Figure 4 summarizes the results of a 1.6 × 1.2 $\mu m^2$ SNOM scan on a Si dewetted island [Fig. 1(a)] of diameter d = 330 nm under the illumination of a supercontinuum source tilted by 30°. The scan step is 50 nm/pixel, and the sub-wavelength spatial resolution of about 200 nm is related to the dimensions of the tip. The normalized near-field spectrum (in purple) collected at the apex of the island is reported in Fig. 4(a), together with the FDTD near-field spectrum acquired at the center of the near-field monitor (in dark green) (details on the normalization of the spectrum are reported in Sec. S5 of the supplementary material). Theoretical and experimental spectra are in good agreement [Fig. 4(a)], allowing us to identify, in the order of decreasing energy, the main higher order multipolar resonances that result from the resonant modes of the antenna with the etalon effect from EH to MQ′. In agreement with the previous assessment of the scattering cross section and near-field spectrum for $\theta = 30°$ shown in FDTD simulations where the two peaks MH′ and EQ spectrally overlap [Fig. 3(b)], the experimental SNOM near-field spectrum at those wavelengths displays a single peak, dominated by the contribution of the EQ resonance [Fig. 4(a)]. Exploiting our HSI technique, we provide the experimental near-field spatial profiles represented in the maps of Fig. 4(b) that are obtained by plotting the intensity integrated around the main peaks in the purple spectrum of Fig. 4(a) [$\lambda = 490$ nm (EH), $\lambda = 530$ nm (MH), $\lambda = 570$ nm (EQ), $\lambda = 645$ nm (MQ), and $\lambda = 735$ nm (MQ′)]. It is worth noting that this spectral analysis might be useful for emission enhancement applications, for example, to match the spectral position of magnetic emissions by trivalent europium.[22]

During a SNOM scan, scattering spectra and morphology of the sample are simultaneously acquired. Thus, we can overlap optical and morphological maps [the island is highlighted by white circles in Fig. 4(b)] and directly compare them with simulations. Experimental and simulated maps show striking similarities in the spatial symmetry of the resonances that are typical of each mode and in the relative weights of the lobes of each mode, indicating preferential directions of scattering [Figs. 4(b) and 4(c)]. The asymmetric "ring crowns" are well reproduced, in terms of intensity, spatial location, and distance from the island. Under tilted illumination, higher-energy modes, such as EH and MH, display a near-field scattered intensity that is unbalanced in the opposite direction with respect to lower energy modes, such as MQ and MQ′ (toward left for EH and MH and toward right for MQ and MQ′). The EQ mode, instead, exhibits a more symmetric distribution both in theory and experiment. The symmetry of EQ is well recognizable in the experimental map, where a vertical dip in the intensity of the signal is visible. In particular, the signal intensity of the MQ′ mode reproduces with high fidelity the expected spatial modulation characterized by a bright lobe on the left side of the island and a clear signal dip on the opposite side.

Deviations between theory and experiment, such as the peak central wavelengths and spectral broadening, and eventual sub-micrometric details not perfectly reproduced in the SNOM maps can be ascribed to several factors: (i) approximation of the island shape as an ideal hemisphere in contrast with a smaller aspect ratio, typical of the equilibrium shape of dewetted silicon;[25] (ii) asymmetries and imperfections of the island shape that did not yet reach its final equilibrium shape;[27,31] (iii) presence of residual Si and intermixing of Si with the underlying $SiO_2$ resulting from the high temperature annealing,[32] producing a strong scattering from the areas nearby the island; (iv) this Si interdiffusion in the $SiO_2$ layer can be schematized with an effective slightly thicker $SiO_2$ substrate with respect to the nominal value of t = 2 $\mu$m, which can affect the etalon


© Author(s) 2021

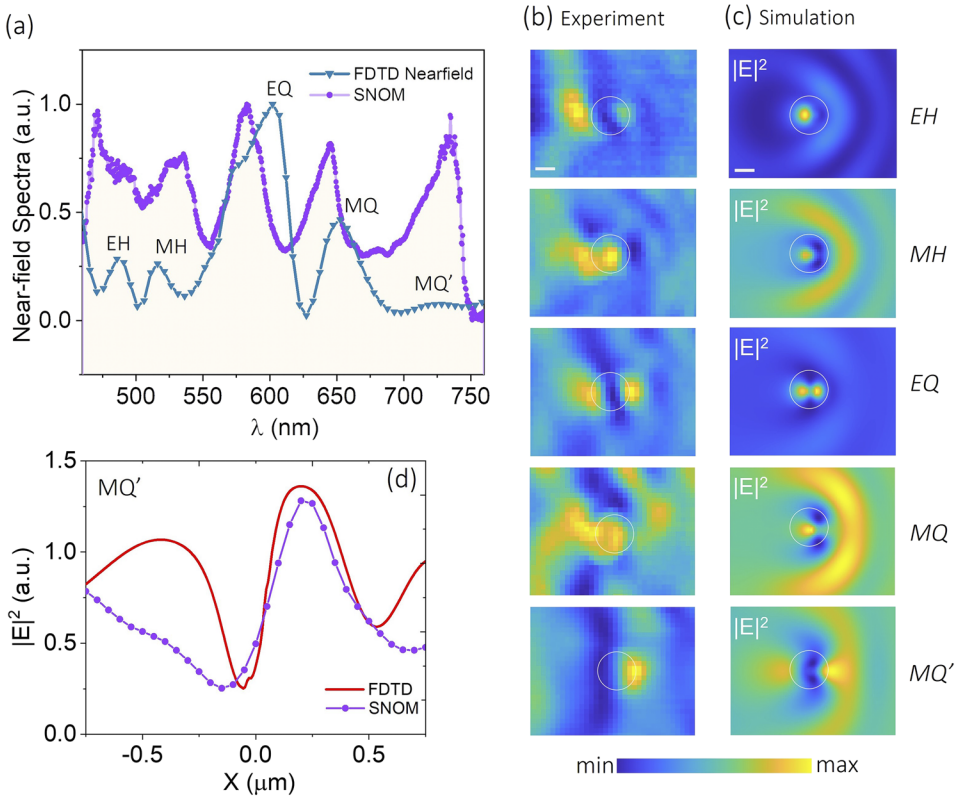


**FIG. 4.** (a) Normalized SNOM scattering spectrum collected on top of the dewetted island of d = 330 nm (purple dots) and FDTD near-field spectrum acquired at a 10 nm distance from the top center of a hemisphere of the same diameter (in dark green). (b) Experimental SNOM maps filtered around the central wavelength of the purple spectrum in (a), respectively, relative to the EH ($\lambda$ = 490 nm), MH ($\lambda$ = 530 nm), EQ ($\lambda$ = 570 nm), MQ ($\lambda$ = 645 nm), and MQ′ $\lambda$ = 735 nm modes. (c) FDTD maps of the electric field intensity of the multipolar resonances detected in the dark green spectrum: EH ($\lambda$ = 485 nm), MH ($\lambda$ = 521 nm), EQ ($\lambda$ = 602 nm), MQ ($\lambda$ = 654 nm), and MQ′ $\lambda$ = 728 nm. All white scale bars correspond to 200 nm. (d) Horizontal cuts along the central part of the experimental and FDTD maps relative to the MQ′ resonance.

peaks position [see Fig. S5(e) of the supplementary material]; and (v) projection of the near-field intensity neglecting the change in tip height during the scan on a 3D object and/or the collection of light form the sides of the optical fiber that modifies the collection efficiency and slightly distorts the reconstructed SNOM optical image. These results show that in the perspective of maximizing the surface enhancement in absorption or in Raman scattering of a single molecule or other quantum system,[3] it is possible to control the absorption of an emitter coupled to the resonator by acting on the electric field hotspot positions induced by the external illumination angle. This might represent an interesting alternative way to the most common approaches in this kind of applications.

In conclusion, we provided a complete near-field hyperspectral imaging study of the modes arising from the combination of the Mie resonances of an all-dielectric dewetted island with the etalon effect due to a thick $SiO_2$ layer below the scatterer. By means of FDTD simulations, we achieved a full comprehension of the sensitivity of magnetic light with respect to the thickness of the substrate and the angle of illumination. The optical characterization of higher order multipolar terms, such as magnetic quadrupoles and hexapoles, can be exploited as an efficient tool to promote the magnetic radiative decay in quantum emitters such as trivalent lanthanide ions in emission enhancement applications. The combination of numerical and experimental results offers a detailed analysis of how such sensitivity affects the near-field scattering pattern of the antenna, suggesting a novel approach to control the position of the localized electric field maxima to engineer an important aspect of the coupling between emitters and antenna: instead of placing the emitter on the hotspot, the hotspot can be moved on the emitter position, offering a versatile tuning tool to control the absorption of the emitter itself.

## SUPPLEMENTARY MATERIAL

See the supplementary material for more details on the simulations process, the experimental setup, and data analysis.

## ACKNOWLEDGMENTS

This research was funded by the EU H2020 FET-OPEN project NARCISO (Grant No. 828890) and the French National Research Agency (ANR) through the projects ULYSSES (Grant


© Author(s) 2021

No. ANR-15-CE24-0027-01) and OCTOPUS (Grant No. ANR-18-CE47-0013-01).

## AUTHOR DECLARATIONS

### Conflict of Interest

The authors have no conflicts to disclose.

## DATA AVAILABILITY

The data that support the findings of this study are available from the corresponding author upon reasonable request.

## REFERENCES

[1] A. I. Kuznetsov, A. E. Miroshnichenko, M. L. Brongersma, Y. S. Kivshar, and B. Luk'yanchuk, "Optically resonant dielectric nanostructures," Science **354**, aag2472 (2016).
[2] I. M. Hancu, A. G. Curto, M. Castro-López, M. Kuttge, and N. F. van Hulst, "Multipolar interference for directed light emission," Nano Lett. **14**, 166–171 (2014).
[3] I. Suárez, T. Wood, J. P. Martinez Pastor, D. Balestri, S. Checcucci, L. David, L. Favre, J. B. Claude, D. Grosso, A. F. Gualdrón-Reyes, I. Mora-Seró, M. Abbarchi, and M. Gurioli, "Enhanced nanoscopy of individual $CsPbBr_3$ perovskite nanocrystals using dielectric sub-micrometric antennas," APL Mater. **8**, 021109 (2020).
[4] N. Dotti, F. Sarti, S. Bietti, A. Azarov, A. Kuznetsov, F. Biccari, A. Vinattieri, S. Sanguinetti, M. Abbarchi, and M. Gurioli, "Germanium-based quantum emitters towards a time-reordering entanglement scheme with degenerate exciton and biexciton states," Phys. Rev. B **91**(20), 205316 (2015).
[5] A. Capretti, A. Lesage, and T. Gregorkiewicz, "Integrating quantum dots and dielectric Mie resonators: A hierarchical metamaterial inheriting the best of both," ACS Photonics **4**, 2187–2196 (2017).
[6] A. Tognazzi, K. I. Okhlopkov, A. Zilli, D. Rocco, L. Fagiani, E. Mafakheri, M. Bollani, M. Finazzi, M. Celebrano, M. R. Shcherbakov, A. A. Fedyanin, and C. De Angelis, "Third-harmonic light polarization control in magnetically resonant silicon metasurfaces," Opt. Express **29**(8), 11605 (2021).
[7] H. Alhalaby, H. Zaraket, and M. Principe, "Enhanced photoluminescence with dielectric nanostructures: A review," Results Opt. **3**, 100073 (2021).
[8] F. Todisco, R. Malureanu, C. Wolff, P. A. D. Gonçalves, A. S. Roberts, N. A. Mortensen, and C. Tserkezis, "Magnetic and electric Mie-exciton polaritons in silicon nanodisks," Nanophotonics **9**(4), 803–814 (2020).
[9] J. Van de Groep and A. Polman, "Designing dielectric resonators on substrates: Combining magnetic and electric resonances," Opt. Express **21**(22), 26285–26302 (2013).
[10] F. Hao and P. Nordlander, "Efficient dielectric function for FDTD simulation of the optical properties of silver and gold nanoparticles," Chem. Phys. Lett. **446**, 115–118 (2007).
[11] P. Spinelli, M. A. Verschuuren, and A. Polman, "Broadband omnidirectional antireflection coating based on subwavelength surface Mie resonators," Nat. Commun. **3**, 692 (2012).
[12] A. B. Evlyukhin, S. M. Novikov, U. Zywietz, R. L. Eriksen, C. Reinhardt, S. I. Bozhevolnyi, and B. N. Chichkov, "Demonstration of magnetic dipole resonances of dielectric nanospheres in the visible region," Nano Lett. **12**, 3749–3755 (2012).
[13] A. I. Kuznetsov, A. E. Miroshnichenko, Y. H. Fu, J. Zhang, and B. Luk'yanchuk, "Magnetic light," Sci. Rep. **2**, 492-1–492-6 (2012).
[14] T. Coenen, J. Van de Groep, and A. Polman, "Resonant modes of single silicon nanocavities excited by electron irradiation," ACS Nano **7**(2), 1689–1698 (2013).
[15] T. G. Habteyes, I. Staude, K. E. Chong, J. Dominguez, M. Decker, A. Miroshnichenko, Y. Kivshar, and I. Brener, "Near-field mapping of optical modes on all-dielectric silicon nanodisks," ACS Photonics **1**, 794–798 (2014).
[16] A. E. Miroshnichenko, A. B. Evlyukhin, Y. F. Yu *et al.*, "Nonradiating anapole modes in dielectric nanoparticles," Nat. Commun. **6**, 8069 (2015).
[17] R. M. Bakker, D. Permyakov, Y. Feng Yu, D. Markovich, R. Paniagua-Domínguez, L. Gonzaga, A. Samusev, Y. Kivshar, B. Luk'yanchuk, and A. I. Kuznetsov, "Magnetic and electric hotspots with silicon nanodimers," Nano Lett. **15**(3), 2137–2142 (2015).
[18] P. Alonso-González, P. Albella, F. Neubrech, C. Huck, J. Chen, F. Golmar, F. Casanova, E. Hueso, A. Pucci, J. Aizpurua, and R. Hillenbrand, "Experimental verification of the spectral shift between near- and far-field peak intensities of plasmonic infrared nanoantennas," Phys. Rev. Lett. **110**, 203902 (2013).
[19] T. Neuman, P. Alonso-González, A. Garcia-Etxarri, M. Schnell, R. Hillenbrand, and J. Aizpurua, "Mapping the near fields of plasmonic nanoantennas by scattering-type scanning near-field optical microscopy," Laser Photonics Rev. **9**, 637–649 (2015).
[20] P. Alonso-Gonzalez, M. Schnell, P. Sarriugarte, H. Sobhani, C. Wu, N. Arju, A. Khanikaev, F. Golmar, P. Albella, L. Arzubiaga, F. Casanova, L. E. Hueso, P. Nordlander, G. Shvets, and R. Hillenbrand, Nano Lett. **11**(9), 3922–3926 (2011).
[21] See http://www.lumerical.com for FDTD Solutions, Lumerical Solutions, Inc.
[22] S. Karaveli and R. Zia, "Strong enhancement of magnetic dipole emission in a multilevel electronic system," Opt. Lett. **35**(20), 3318–3320 (2010).
[23] B. Rolly, B. Bebey, S. Bidault, B. Stout, and N. Bonod, "Promoting magnetic dipolar transition in trivalent lanthanide ions with lossless Mie resonances," Phys. Rev. B **85**, 245432 (2012).
[24] C. V. Thompson, "Solid-state dewetting of thin films," Annu. Rev. Mater. Res. **42**(1), 399–434 (2012).
[25] D. Toliopoulos, M. Khoury, M. Bouabdellaoui, N. Granchi, J.-B. Claude, A. Benali, I. Berbezier, D. Hannani, A. Ronda, J. Wenger, M. Bollani, M. Gurioli, S. Sanguinetti, F. Intonti, and M. Abbarchi, "Fabrication of spectrally sharp Si-based dielectric resonators: Combining etaloning with Mie resonances," Opt. Express **28**(25), 37734–37742 (2020).
[26] M. Abbarchi, M. Naffouti, B. Vial, A. Benkouider, L. Lermusiaux, L. Favre, A. Ronda, S. Bidault, I. Berbezier, and N. Bonod, "Wafer scale formation of monocrystalline silicon-based Mie resonators via silicon-on-insulator dewetting," ACS Nano **8**(11), 11181–11190 (2014).
[27] M. Naffouti, R. Backofen, M. Salvalaglio, T. Bottein, M. Lodari, A. Voigt, T. David, A. Benkouider, I. Fraj, L. Favre, A. Ronda, I. Berbezier, D. Grosso, M. Abbarchi, and M. Bollani, "Complex dewetting scenarios of ultrathin silicon films for large-scale nanoarchitectures," Sci. Adv. **3**(11), eaao1472 (2017).
[28] E. D. Palik, *Handbook of Optical Constants of Solids* (Academic, 1985).
[29] N. A. Butakov and J. A. Schuller, "Designing multipolar resonances in dielectric metamaterials," Sci. Rep. **6**, 38487 (2016).
[30] J. Berzins, S. Indrisiunas, K. Van Erve, A. Nagarajan, S. Fasold, M. Steinert, G. Gerini, P. Gecys, T. Pertsch, S. M. B. Baumer, and F. Setzpfandty, "Direct and high-throughput fabrication of Mie resonant metasurfaces *via* single-pulse laser interference," ACS Nano **14**(5), 6138–6149 (2020).
[31] M. Bollani, M. Salvalaglio, A. Benali *et al.*, "Templated dewetting of single-crystal sub-millimeter-long nanowires and on-chip silicon circuits," Nat. Commun. **10**, 5632 (2019).
[32] F. Leroy, Y. Saito, S. Curiotto, F. Cheynis, O. Pierre-Louis, and P. Müller, "Shape transition in nano-pits after solid-phase etching of $SiO_2$ by Si islands," Appl. Phys. Lett. **106**, 191601 (2015).


© Author(s) 2021